FFI Norwegian Defence Research Establishment

23/00043

FFI-RAPPORT

Analysis of multirotor drone wind response

Øistein Thomle Hoelsæter

Analysis of multirotor drone wind response

Øistein Thomle Hoelsæter

Norwegian Defence Research Establishment (FFI) 20 March 2023

Keywords
Droner
Modellering og simulering
Styring og kontroll
Vind
Vær

FFI report
23/00043

Project number
1493

Electronic ISBN
978-82-464-3464-3

Approvers
Halvor Bjordal, *Research Manager*
Halvor Ajer, *Director of Research*

The document is electronically approved and therefore has no handwritten signature.

Summary

This report describes the fundamental mechanisms and response of a generic multirotor drone when subjected to gusting wind. We have used simplified dynamic models, both linear and nonlinear. Based on these, we have analyzed horizontal position deviations. The models were also used to understand the effect of changes in parameters like mass, inertial moments, drag and control system strategy. The study has a qualitative view. The simulation examples are not representative for a specific type or class of multirotor drones.

Sammendrag

Denne rapporten beskriver de grunnleggende mekanismene og responsen til en generisk multirotordrone når den utsettes for varierende vind. Vi har brukt forenklede dynamiske modeller, både lineære og ulineære. Ut fra dem har vi analysert horisontale posisjonsavvik. Modellene er også brukt for å forstå effekten av endringer i parametere som masse, treghetsmomenter, drag og kontrollsystemstrategi. Studien legger vekt på det kvalitative. Simuleringseksemplene er ikke representative for en bestemt type eller klasse av multirotordroner.

Contents

1 Introduction

The multirotor drone concept was introduced to the toy market about the year 2005 and to the more professional market a few years later. The first models had limited maneuverability and was relatively sensitive to wind. The fixed pitch propeller and the control principle of constantly changing the motor rpms were believed by many to limit the future usefulness of the concept.

Technological advances in computing power, inertial measurement sensors and GPS, brushless motors and motor controllers, batteries and extremely low weight propellers and airframes have contributed to the now widespread use of drones, both as recreational toys and for professional use.

The use of larger drones for logistics purposes are now becoming more feasible. FFI has been participating in a project investigating the possible use of drones for medical logistics, more specific for transportation of blood samples and human organs. It is a requirement for such a system to operate in almost all kinds of weather, and to be able to land and take off from tall buildings in an urban environment.

Modern multirotor drones are known for being very robust with respect to wind resistance. Due to the expected turbulent wind conditions in an urban environment, there has been a concern how a heavy loaded drone will cope with gusting wind during take-off and landing.

The intention of this study is not to answer the question if and under which windy conditions a logistics drone can perform safely. The intention has been to establish a better understanding of the basic physics involved when a drone is exposed to wind as well as the importance of key parameters of the drone and its control system.

The modeling of the aerodynamics in this study is not very sophisticated. The study must therefore be regarded as more of a qualitative than quantitative nature. However, it is believed that the position deviations found as a function of wind influence is indicative of what can be expected in real life.

Note also that the study focuses on horizontal position deviations only, as this is assumed to be the most important during take-off and landing.

The drone model used in the study is inspired by the DJI Matrice 600. However, it is not a direct or detailed modeling of this exact drone. FFI has practical experience with this drone, and the use of DJI Matrice 600 as a template makes it possible to compare the simulations with real world wind response measurements at a later stage.

All simulations have been performed by using a mix of Matlab scripting and the Simulink graphical simulation tool.

Figure 1.1 DJI Matrice 600 drone with a test payload for medical logistic services

2 Simplified linear model

2.1 Modeling

To be able to perform a theoretical analysis of how different parameters influences the wind response of a drone, a simplified (pitch plane only), linear model of the drone and its control system is defined. In chapter 3, simulations with a more realistic, nonlinear model is performed.

When a system qualifies as a *linear system*, it is possible to use the responses to a small set of inputs to predict the response to any possible input [1]. In our linearized model, the response to a small wind disturbance can then be scaled to find the response to any wind input. This is of course a simplification, but enables an analytical analysis of the system in the region around the linearization condition.

To counter the effects of wind, the basic control principle of a multirotor drone is to tilt the drone a pitch angle θ so that the horizontal force component F_h equals the drag D. To tilt the drone, a moment is applied by differentiating the thrust on the fore and aft motors. This moment acts through the drone moment of inertia and results in an angular acceleration. The resulting pitch angle dynamics is a function of several factors like pitch angle controller tuning, propeller weight, motor arm length, available power as well as drone moment of inertia.

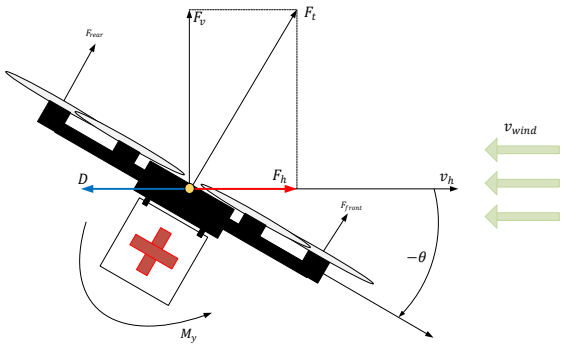

Figure 2.1 Basic force arrangement for a drone hovering in wind

To be able to suppress the wind disturbance, the drone must employ a position controller. The position controller used in the analysis is a typical PID-controller with the following Laplace-representation:

$$G_{pc}(s) = (P + Ds + \frac{I}{s}) \tag{2.1}$$

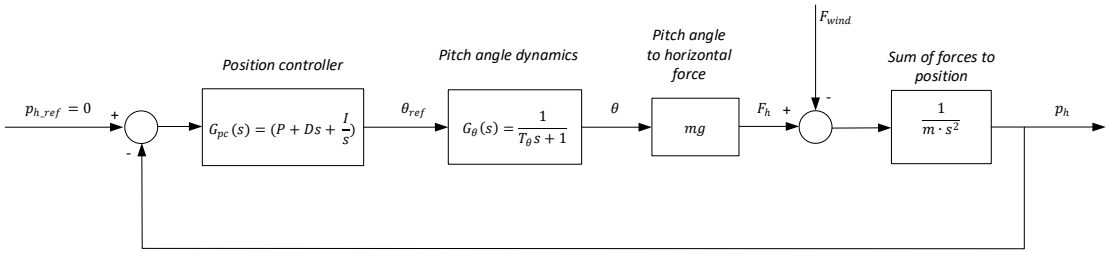

Figure 2.2 Simplified structure for drone and control system subjected to a wind disturbance

The output from the PID-controller is a pitch angle demand $\theta_{ref}(s)$. The pitch angle dynamics is very simplified modeled as a first order model with time constant T_θ. This is a "black box" modeling approach which sums up all the effects of propeller inertia, motor torque, propeller thrust, motor arm lengths, drone moments of inertia as well as the pitch angle controller tuning into the single parameter T_θ.

$$G_\theta(s) = \frac{\theta(s)}{\theta_{ref}(s)} = \frac{1}{T_\theta s + 1} \tag{2.2}$$

The pitch angle to horizontal force relation is modeled as:

$$F_h = F_v \cdot tan(\theta) = m \cdot g \cdot tan(\theta) \tag{2.3}$$

$$\frac{dF_h}{d\theta} = m \cdot g \cdot \frac{1}{cos^2(\theta)} \quad (2.4)$$

The system is then linearized at pitch angle $\theta = 0°$ which is the condition for hovering in no wind.

$$G_F(s) = \frac{F_h(s)}{\theta(s)} = mg \quad (2.5)$$

(2.5) is in the linear model analysis assumed to be valid for small pitch angles θ.

The transition from the sum of forces to position displacement:

$$p_h = \frac{1}{m}\iint (F_h - F_{wind})dt \quad (2.6)$$

$$p_h(s) = \frac{1}{ms^2}(F_h(s) - F_{wind}(s)) \quad (2.7)$$

To be able to analyze the wind response, the transfer function in Figure 2.1 is rearranged so that the wind force F_{wind} (aerodynamic drag) becomes the input and position deviation p_h becomes the output.

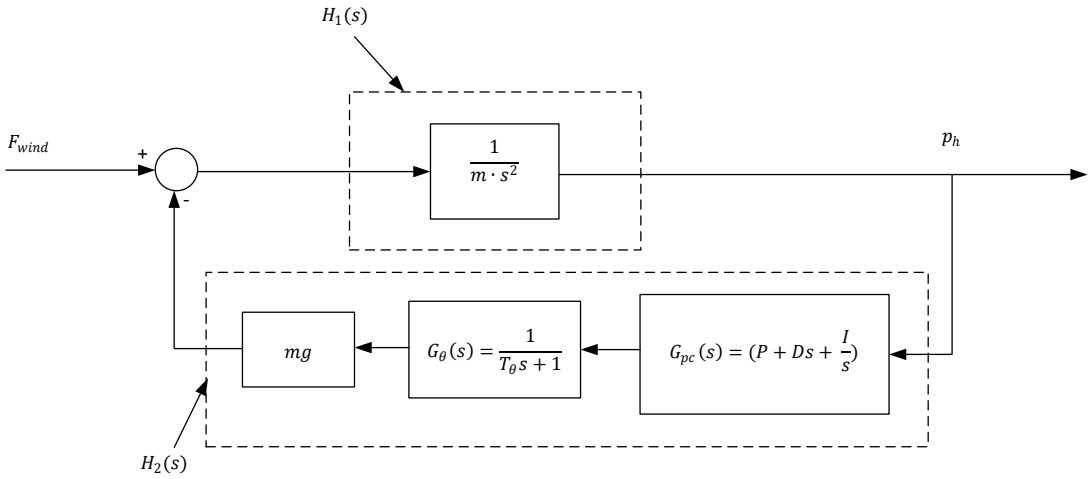

Figure 2.3 Rearranged block diagram for analyzing the position response to a wind force input

Using theory for negative feedback closed loop systems; the transfer function from wind force to position deviation (the block diagram in Figure 2.2) can be simplified and found to be:

$$G_{wp}(s) = \frac{p_h(s)}{F_{wind}(s)} = \frac{H_1(s)}{1+H_1(s)H_2(s)} = \frac{T_\theta s^2+s}{mT_\theta s^4+ms^3+k_\theta Ds^2+k_\theta Ps+k_\theta I} \quad (2.8)$$

The denominator is of 4th order and can be factorized into two second order systems with the natural frequencies ω_1 and ω_2 and corresponding damping ratio ζ_1 and ζ_2. Dividing the numerator and denominator by mT_θ, $G_{wp}(s)$ can now be written as:

$$G_{wp}(s) = \frac{\frac{1}{m}(s^2+s)}{s^4+\frac{1}{T_\theta}s^3+\frac{k_\theta D}{mT_\theta}s^2+\frac{k_\theta P}{mT_\theta}s+\frac{k_\theta}{mT_\theta}I} = \frac{\frac{1}{m}(s^2+s)}{(s^2+2\zeta_1\omega_1 s+{\omega_1}^2)(s^2+2\zeta_2\omega_2 s+{\omega_2}^2)} \quad 2.9)$$

The denominator of $G_{wp}(s)$ can be expanded to:

$$s^4 + (2\zeta_2\omega_2)s^3 +$$

$$({\omega_2}^2)s^2 + (2\zeta_1\omega_1)s^3 + (4\zeta_1\omega_1\zeta_2\omega_2)s^2 + (2\zeta_1\omega_1{\omega_2}^2)s + ({\omega_1}^2)s^2 +$$

$$(2\zeta_2\omega_2{\omega_1}^2)s + {\omega_1}^2{\omega_2}^2 \quad (2.10)$$

=

$$\boldsymbol{s^4} + \boldsymbol{s^3}[2\zeta_2\omega_2 + 2\zeta_1\omega_1] + \boldsymbol{s^2}[{\omega_2}^2 + 4\zeta_1\omega_1\zeta_2\omega_2 + {\omega_1}^2] +$$

$$\boldsymbol{s}[2\zeta_1\omega_1{\omega_2}^2 + 2\zeta_2\omega_2{\omega_1}^2] + [\,{\omega_1}^2{\omega_2}^2] \quad (2.11)$$

→

$$\frac{1}{T_\theta} = 2\zeta_2\omega_2 + 2\zeta_1\omega_1 \quad (2.12)$$

$$\frac{k_\theta D}{mT_\theta} = \frac{gD}{T_\theta} = {\omega_2}^2 + 4\zeta_1\omega_1\zeta_2\omega_2 + {\omega_1}^2 \quad (2.13)$$

$$\frac{k_\theta P}{mT_\theta} = \frac{gP}{T_\theta} = 2\zeta_1\omega_1{\omega_2}^2 + 2\zeta_2\omega_2{\omega_1}^2 \quad (2.14)$$

$$\frac{k_\theta I}{mT_\theta} = \frac{gI}{T_\theta} = {\omega_1}^2{\omega_2}^2 \quad (2.15)$$

The four equations (2.12) to (2.15) show how the natural frequencies and the corresponding relative damping are related to the properties of the drone and its control system. Further solving to find explicit expressions for the natural frequencies and corresponding damping is outside the scope of this report.

However, from the equations above it is possible to extract the following findings:

1. The natural frequencies and their damping ratio is invariant to vehicle mass itself. However, *mass distribution* is a parameter influencing the pitch angle dynamics (T_θ), and therefore influencing the natural frequencies.

2. The position response to wind disturbances in inversely proportional to vehicle mass (assuming constant pitch angle dynamics and position controller parameters). This can be seen from the $\frac{1}{m}$ term in the numerator of $G_{wp}(s)$.

2.2 Wind response - frequency analysis

To validate the analysis and findings in chapter 2.1, a typical frequency analysis was performed. *s* is then substituted with $j\omega$ in the simplified linear model:

$$G_{wp}(j\omega) = \frac{p_h(j\omega)}{F_{wind}(j\omega)} = \frac{T_\theta(j\omega)^2+(j\omega)}{mT_\theta(j\omega)^4+m(j\omega)^3+k_\theta D(j\omega)^2+k_\theta P(j\omega)+k_\theta I} \quad (2.16)$$

where $k_\theta = mg$

Nominal parameters were set to:

m = [8 10 12 14 16] kg

$T_\theta = 0.1\ sec$

P = 0.8

D = 0.5

I = 0.4

Note that in this simplified analysis, wind is treated as a disturbing *force*, not as air moving at a given velocity. Therefore, the output of the system is a position deviation measured in meters, and the input is a force measured in Newton. The relation between wind speed and disturbing force will be included in the more complex nonlinear model in chapter 3.

In the following plots, $f_1 = \frac{\omega_1}{2\pi}$ and $f_2 = \frac{\omega_2}{2\pi}$ are indicated in the plots.

The *bode*-function in Matlab was used to compute the following frequency response of $G_{wp}(j\omega)$:

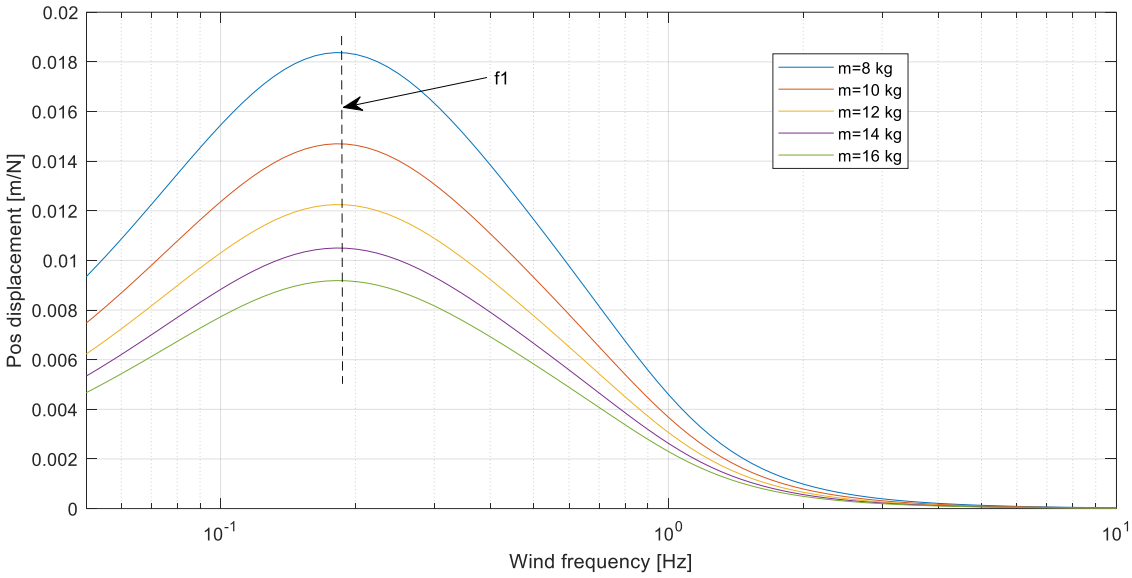

Figure 2.4 Frequency response as function of vehicle mass. First natural frequency is as expected from the analysis invariant to vehicle mass.

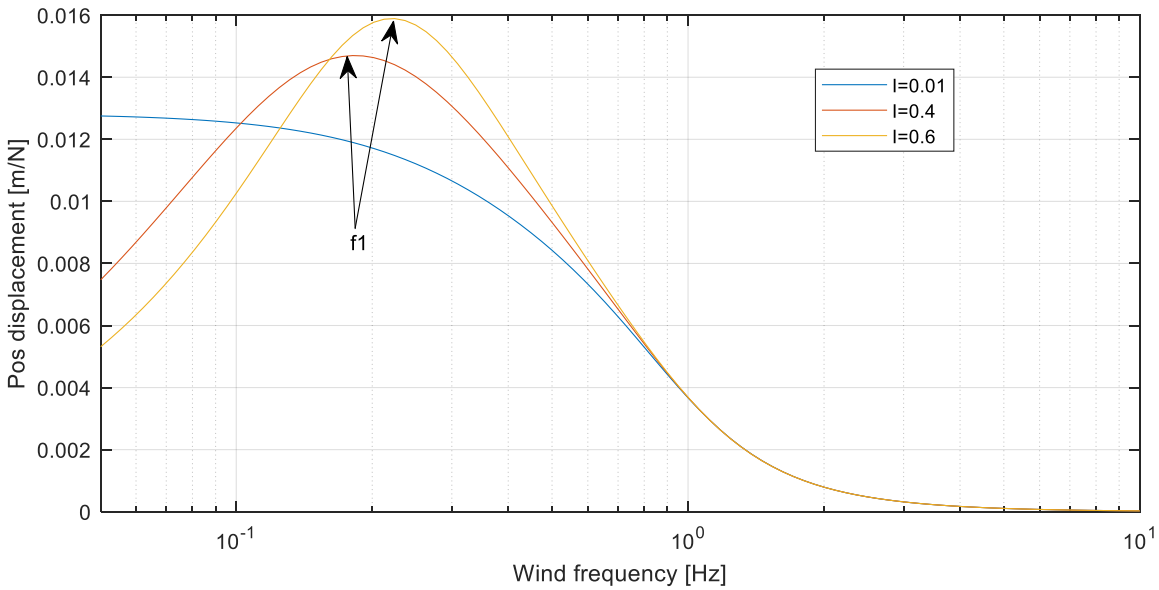

Figure 2.5 Frequency response as a function of controller integral term I (m=10kg). Low frequency attenuating effect of I-term is obvious. f_1 is increasing with I-term.

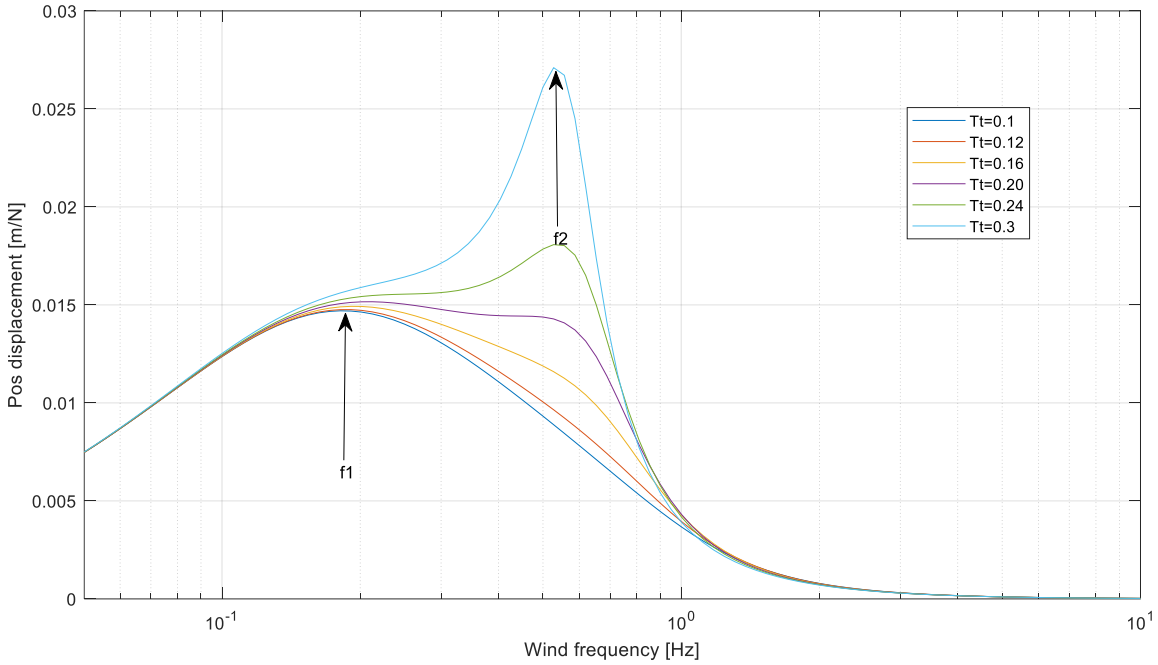

Figure 2.6 Effect of increasing the pitch angle response time T_θ = 0.1 → 0.3 sec

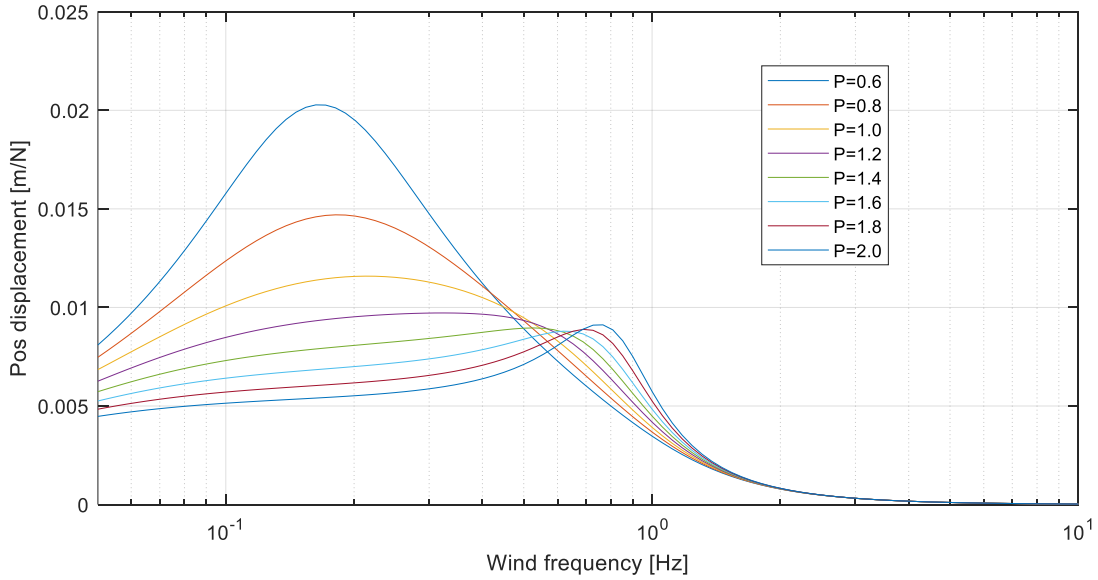

Figure 2.7 Effect of increasing the proportional gain P = [0.6→2.0]. In a nonlinear system, with saturations and other constraints, increasing the P-term this much might cause instability.

3 More complex nonlinear model

In this chapter, a more detailed analysis of the wind response will be performed using a more complex and nonlinear model of a drone. As described in chapter 1, the drone model is inspired by the size and other characteristics of the DJI Matrice 600. It is however not an exact representation of this drone.

3.1 Airframe configuraton

The airframe modeled is a conventional hexacopter with the motor layout as shown in Figure 3.1. With this layout, the two motors aligned with the y_b-axis only contributes to the total thrust. The 4 other motors (front and rear) are used for total thrust as well as for generating differential thrust for pitch angle control.

The center body section is assumed to contain the flight controller and other avionics as well as the batteries. An underslung payload is mounted as shown in Figure 3.2.

The drone is assumed to have a lightweight, rectractable landing gear and the low mass and inertia of this is not included in the model.

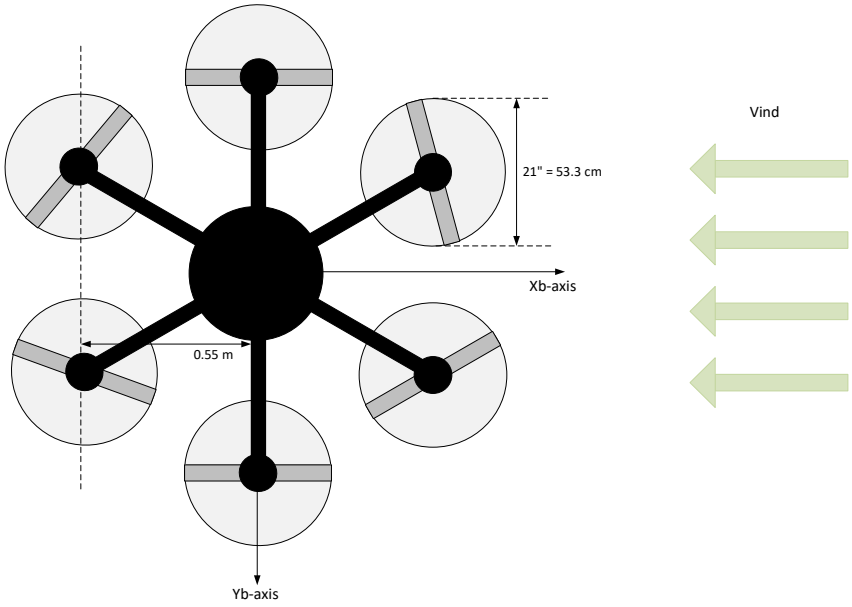

Figure 3.1 Drone airframe configuration as seen from above

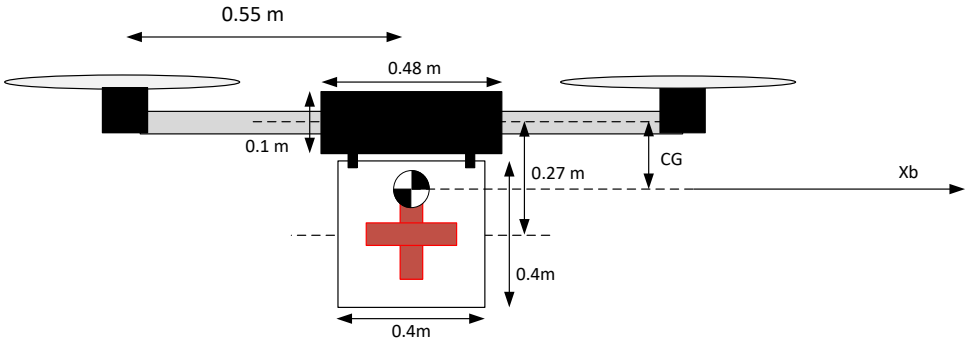

Figure 3.2 Configuration of the drone with underslung payload

3.1.1 Inertial properties

The central body of the drone is modeled as a disc with mass m_{body} (variable), radius $r_{body} = 0.24\ m$ and height $h_{body} = 0.1\ m$.

Each of the motors has a mass of $m_{motor} = 0.315$ kg. The front and rear motors are offset a distance $x_{motor} = 0.55\ m$ from the center of the body.

The payload is modeled as a cube with mass $m_{pload} = 4.5\ kg$, size $l_{pload} = 0.4m$, and its center of mass is offset a distance $z_{pload} = 0.27m$ from the arms is indicated in Figure 3.2.

In this study, the weight of the payload is kept constant. When varying the total mass of the drone in the later chapters, this is done by altering the mass of the central body section (as if using different size batteries). This is to avoid too much change in the moments of inertia of the drone, and the possible need for a time consuming retuning of the control system.

The vertical location of the center of gravity of the drone, z_{CG} (relative to the center of the arm tubes), can be calculated as:

$$z_{cg} = \frac{m_{pload} \cdot z_{pload}}{m_{drone}} \tag{3.1}$$

The moments of inertia for rotation about the I_y −axis (going through CG) were calculated using standard formulas for common shaped objects [4], and the parallel axis theorem (also known as the *Huygens-Steiner* theorem):

$$I_{y\_motors} = 4 \cdot m_{motor} \cdot {x_{motor}}^2 + 6 \cdot\ m_{motor} \cdot {z_{cg}}^2$$

$$I_{y\_arms} = 2 \cdot (\frac{1}{12} m_{arm} \cdot {l_{arm}}^2) + 3 \cdot\ m_{arm} \cdot {z_{cg}}^2$$

$$I_{y\_body} = \frac{1}{12} m_{body} \cdot (3{r_{body}}^2 + {h_{body}}^2) + m_{body} \cdot {z_{cg}}^2$$

$$I_{y\_pload} = \frac{1}{6} m_{pload} \cdot {l_{pload}}^2 + m_{pload} \cdot (z_{pload} - z_{cg})^2$$

$$I_{y\_drone} = I_{y\_motors} + I_{y\_arms} + I_{y\_body} + I_{y_{pload}} = 0.84\ kgm^2 \quad (3.1)$$

3.2 Modeling of drag

Precise modeling of drag is very complex, especially for an object like a multirotor drone. Most theory and tools for drag estimation is more suited for a fixed wing airplane with more or less standard wing panels and a streamlined fuselage.

This study is mostly of a qualitative nature and we can therefore do some coarse assumptions regarding the modeling of drag.

We assume that the drag acting on the drone can be modeled as a base drag plus a drag component that increases as the drone is tilted (changing the pitch angle θ increases the exposed frontal area).

$$k_a = \frac{1}{2} \sigma {v_{air}}^2 S \quad (3.2)$$

$$D = k_a(Cd_0 + Cd_\theta\, |sin\,\theta\,|) \quad (3.3)$$

Where

$\sigma = 1.225\ Kg/m^3$ (air density)

v_{air} = relative air speed

S = reference area

For helicopters, the rotor disc area is usually used as the reference area *S* [2].

In our case, using 6 propellers with 21" diameter, the reference area then becomes:

$$S = 6\left(\pi \cdot {r_{prop}}^2\right) = 6(\pi \cdot (0.267m)^2) = 1.34\ m^2 \quad (3.4)$$

At constant relative air speed and constant altitude, the drag force D equals the horizontal component of the total trust. If we assume no aerodynamic lift being generated at any pitch angle, the horizontal thrust component can then be expressed:

$$F_h = F_t\ sin\,\theta = \frac{mg}{cos\,\theta} sin\,\theta = mg\ tan\,\theta \quad (3.5)$$

where F_t is total thrust along the drone z_b-axis.

We now make a set of important but rough assumptions:

-The drone has an air speed $v_{max} = 20\ m/s$ at a pitch angle $\theta = -30°$.

-The drag force at pitch angle $\theta = -45°$ is doubled compared to when $\theta = 0°$.

$$D(\theta = 0°) = D_0 = k_a C_{d0} \quad \textit{(drag at pitch angle } \theta = 0°\textit{)} \tag{3.6}$$

$$D(\theta = 45°) = D_{45} = k_a(C_{d0} + \frac{C_{d\theta}}{\sqrt{2}}) \quad \textit{(drag at pitch angle } \theta = 45°\textit{)} \tag{3.7}$$

$$k_a\left(C_{d0} + \frac{C_{d\theta}}{\sqrt{2}}\right) = 2k_a C_{d0} \textit{ (drag at 45° is doubled compared to 0°)} \tag{3.8}$$

$$C_{d\theta} = \sqrt{2}C_{d0} \tag{3.9}$$

At constant velocity, drag equals the horizontal thrust force:

$$\frac{1}{2}\sigma {v_{air}}^2 S\left(Cd_0 + \sqrt{2}C_{d0}sin(\theta)\right) = mg\ tan(\theta) \tag{3.10}$$

Inserting values for the maximum velocity condition, $\theta = 30°$ and $v_{air} = 20\ {}^{m}/_{s}$:

$$C_{d0} = \frac{mg}{\sigma {v_{air}}^2 S(1+\frac{\sqrt{2}}{2})} = 0.121 \tag{3.11}$$

$$C_{d\theta} = \sqrt{2}C_{d0} = 0.172 \tag{3.12}$$

These drag coefficient values are then used in $D = k_a(Cd_0 + Cd_\theta |sin\,\theta|)$ (3.3) to calculate the resulting drag force.

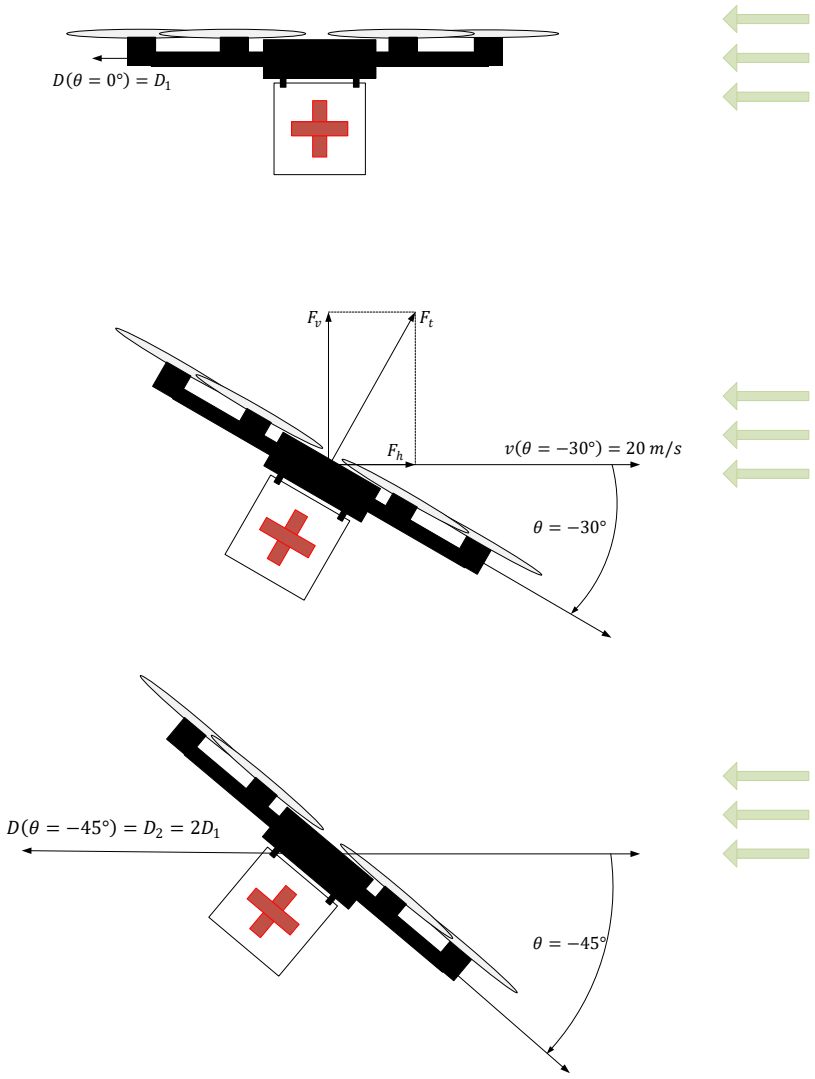

Figure 3.3 Assumptions used to establish a model of the airframe drag force

3.2.1 Nonlinear effects and controllability

Acceleration of the drone in the horizontal plane and relative to the ground is determined by the mass and the difference between the drag force and the horizontal component of the propeller thrust. As described in previous chapters, drag is assumed to be increasing when the drone is tilted. The same applies of course for the horizontal component of propeller thrust. It is increasing with increased tilt as can be seen in Figure 3.3.

It is therefore a strong coupling between the control input (pitch angle θ) used to counter the disturbing wind, and the effect (drag *D*) the disturbance itself (wind) has on the drone. This is an effect not addressed in the previous linear analysis.

Controllability is often referred to as the ability of an input variable to move the output from any initial condition to any final condition in a finite time interval. In this case we are applying pitch angle changes (control input) on a wind influenced drone to control its ground referenced acceleration, velocity and position.

When using pitch angle to counter the wind disturbance, one requirement for controllability will be that changes in the pitch angle must always result in more increase in the horizontal component of the thrust than the increase in drag.

This can be analyzed by comparing the partial derivative of D and F_h with respect to θ.

$$\frac{\partial D}{\partial \theta} = \frac{\partial(\frac{1}{2}\sigma v^2 S(Cd_0 + Cd_\theta \sin\theta))}{\partial \theta} = \frac{1}{2}\sigma v^2 S Cd_\theta \cos\theta \qquad (3.13)$$

$$\frac{\partial F_h}{\partial \theta} = \frac{\partial(mg\tan\theta)}{\partial \theta} = \frac{mg}{(\cos(\theta))^2} \qquad (3.14)$$

$$K_h = \frac{mg}{(\cos(\theta))^2} - \frac{1}{2}\sigma v^2 S Cd_\theta \cos\theta \qquad (3.15)$$

K_h must be > 0 to make the system controllable.

As can be seen from Figure 3.4, using the described drag parameters, the change in net horizontal force as a function of pitch angle θ is always positive and increasing. This indicates that the open loop gain is approximately doubled at $\theta = 40°$ compared to when $\theta = 0°$. In a real world control system implementation, this nonlinearity should probably be accounted for using some sort of gain scheduling. This has however not been utilized in this study as all control loops have constant parameter settings.

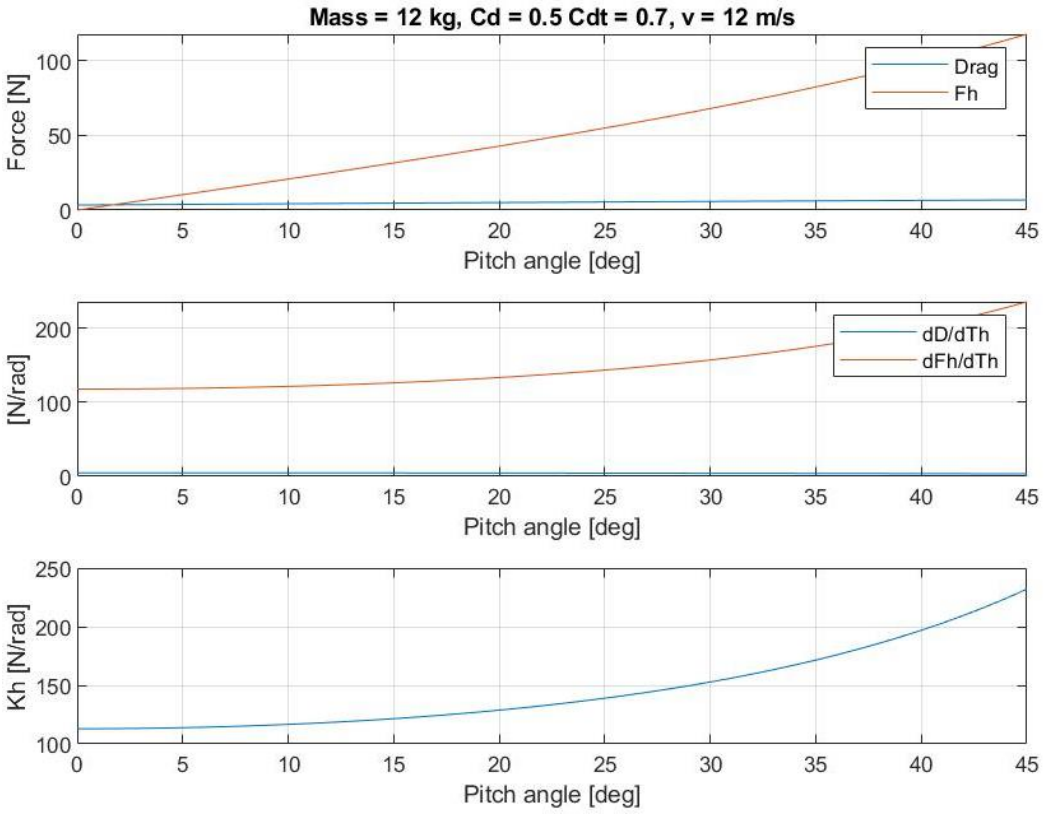

Figure 3.4 Forces and derivatives as function of pitch angle θ

3.3 Modeling of thrust

3.3.1 Propeller

For calculating thrust as a function of rpm as well as power input, one of several available propeller calculators found on the internet was used. These calculators are for the most part developed and used by drone and model airplane enthusiasts, and the accuracy cannot be validated without doing real world measurements.

However, based on our own experience they seem to be not very far off and reflects the expected nonlinear behavior. Data for a typical and generic 21-7 inch (21 diameter – 7 pitch) was generated using the software found at: *https://rcplanes.online/calc_thrust.htm.*

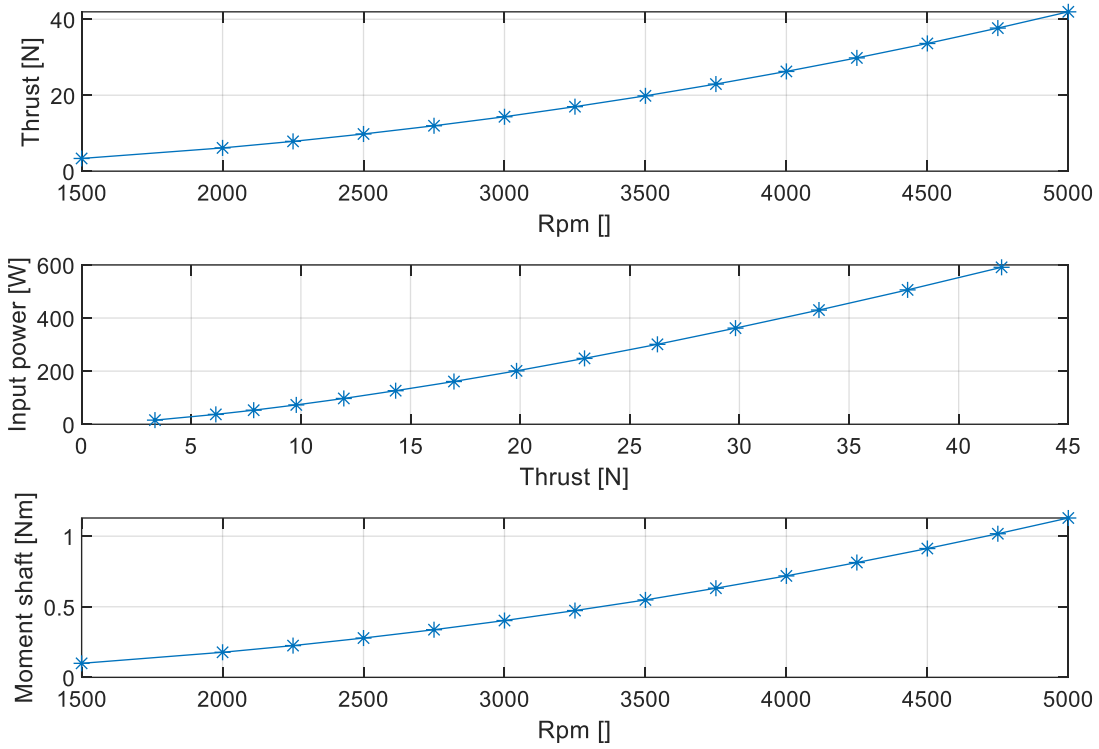

Figure 3.5 Data for generic 21-7 inch propeller

The data generated by the calculator is valid for static thrust only. In practical terms that means that the drone is hovering in no wind. When exposed to horizontal maneuvers and/or wind, the thrust curve will be different from the one calculated for a static situation. The flow into the propeller disc will no longer be perpendicular to the disc plane, and the propeller blade angle of attack will be changed (reduced) due to the drone movements.

Using static thrust data for all drone air speeds is therefore an error source in this study.

3.3.2 Motor, propeller and inertia

We are assuming the use of a lightweight carbon propeller with the size 21”-7”. The propeller mass is $m_{prop} = 0.035$ kg.

The geometry of the propeller is simplified modeled to be a uniform rod. The approximate moment of inertia of the propeller can then be calculated:

$$I_{xx\_p} = \frac{1}{12}\left(m_{prop} \cdot \left(l_{prop}\right)^2\right) = 8.3 \times 10^{-4} kgm^2 \quad (3.16)$$

The rotational dynamics of the rotating mass can then be expressed as:

$$\dot{\omega}_{prop} = \frac{M_{motor}}{I_{xx\_p}} \quad (3.17)$$

where M_{motor} is motor torque.

$$\omega_{prop} = \omega_{prop\_0} + \int \frac{M_{motor}}{I_{xx\_p}}\, dt \quad (3.18)$$

The shaft power of the motor:

$$P_{shaft} = M_{motor} \cdot \omega_{prop} \quad (3.19)$$

The electrical power input to the motor:

$$P_{motor\_IN} = \frac{P_{shaft}}{n_{motor}} = U_{motor} \cdot I_{motor} \quad (3.20)$$

n_{motor} is motor efficiency and assumed to be constant = 0.8 in this study.

3.4 Modeling of aerodynamic pitch stability

Unless otherwise noted, all results from simulations are for a drone model with neutral aerodynamic pitch stability. This means that as the drone is pitching, resulting in a non-zero angle of attack, no positive or negative pitching moment is generated.

3.5 Saturations and nonlinear elements

The following saturation values are implemented in the simulation model :

$|\theta_{max}| = 50°$ (max pitch angle)

$\left|\dot{\theta}_{max}\right| = \frac{3\pi}{2}\ rad/s$ (max pitch angular rate)

$F_{m\_min} = 3.5N$ (min thrust per motor)

$F_{m\_max} = 43N$ (max thrust per motor)

$M_{max} = 1.6Nm$ (max torque for each motor)

3.6 Control system

Note that all models and simulations in this study is valid for horizontal wind only. The wind vector is assumed to have no vertical component and is always in the $x_b - z_b$ plane (see Figure 3.1).

In the simulations, the drone has no active altitude control loop and any effects on altitude from horizontal wind is not analyzed. Instead of an altitude control loop using negative feedback, the total thrust applied to the drone is a feed forward term that is calculated so that the vertical component always equals the mass of the drone:

$$F_t = \frac{mg}{cos(\theta)} \tag{3.21}$$

The lack of an altitude controller will make the drone drift slowly away in the vertical direction, as small errors in the force feed forward accumulates. The vertical behavior is however not addressed in this study, so this is not considered as a problem.

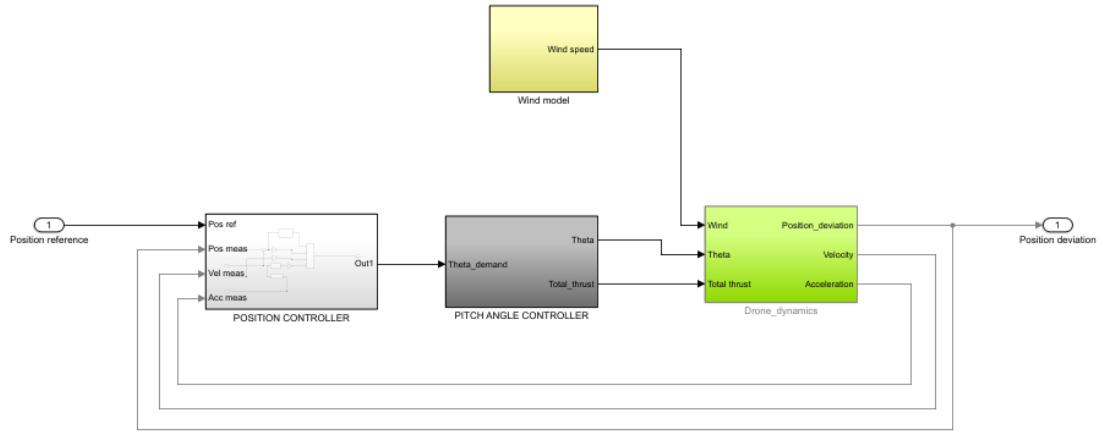

Figure 3.6 Simulator structure for the wind response analysis

3.6.1 Position control loop

The drone control system used in this analysis consists of several nested control loops.

The position controller has a reference position input. In this study it is always zero as if the drone is commanded to hover at a given position. The position controller is using measurements of horizontal acceleration ($\tilde{a}_h$), velocity and position. These measurements are all assumed to have no noise or errors. The position controller is a typical PID-controller, with an additional term being the pitch angle θ_{wc} that in theory will exactly cancel the wind force.

$$\theta_{wc} = sin^{-1}\left(\frac{\tilde{a}_h}{\sqrt{(\tilde{a}_h)^{2+}\, g^2}}\right) \qquad (3.22)$$

Feedback of horizontal velocity v_h is the D-term, and position feedback is the P-term. The I-term is necessary to achieve zero stationary position error from a constant wind disturbance.

Tuning of the PID-parameters was done by qualified trial and error, focusing on the fastest possible response without saturating the control inputs. No gain scheduling was employed.

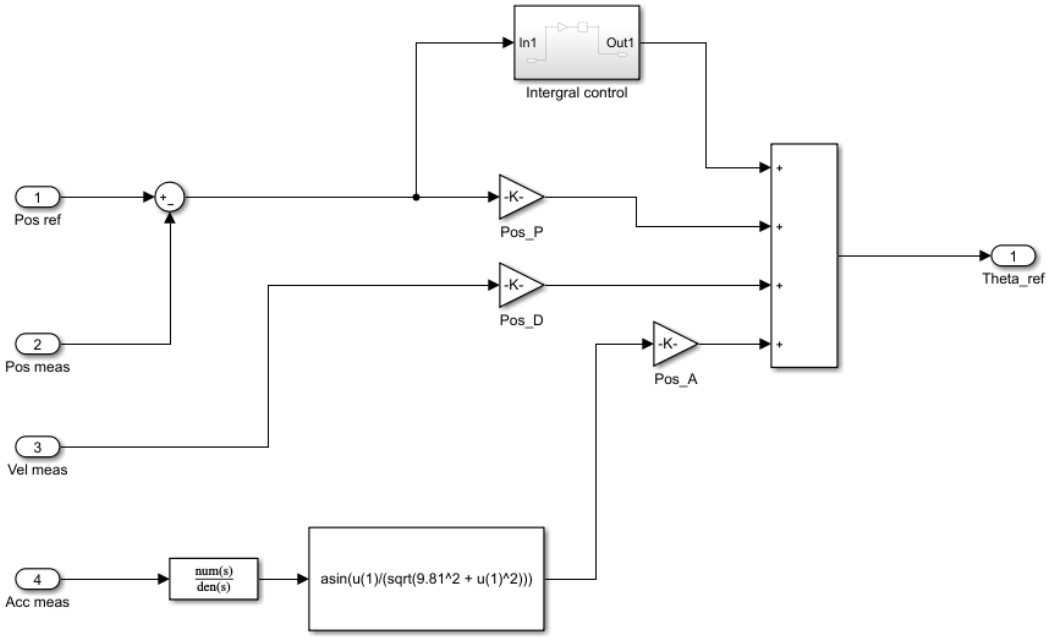

Figure 3.7 Structure of the position controller

3.6.2 Pitch angle control loop

The output from the position controller is a pitch angle demand (to counter the wind influence). The pitch angle controller is demanding individual thrust from the six motors in order to create a moment about the y_b-axis. Thrust from each of the motors are controlled indirectly through a rpm governor. This is explained in more detail in the next chapter.

As was found in the linear analysis, the pitch angle response is very important for the wind suppressing characteristics of the drone. The pitching moment of inertia as well as the thrust response time of the motor/propellers should therefore be kept as low as possible. Increasing the mass of an off-center payload will increase the moments of inertia and give a less damped behavior, especially if the pitch angle controller is not tuned to the new conditions.

For pitch angle control, a PD-controller was implemented. There is no need for an I-term as no external aerodynamic pitching moments (disturbances) are modeled into the drone dynamics. This is the equivalent to having always neutral pitch stability in a fixed wing airplane. With no disturbing moments, zero stationary pitch angle error will be achieved with the integral term I=0.

An example of the frequency response of the pitch angle control loop is shown in Figure 3.8. This plot is the result of simulation of the nonlinear model at 40 discrete frequencies. The plot shows that the 3dB amplitude bandwidth of the pitch angle control loop is in the order of 0.9 Hz.

In practical terms this means that for frequencies above this bandwidth, the control systems ability to counter the wind forces (using pitch angle as control input) are reduced.

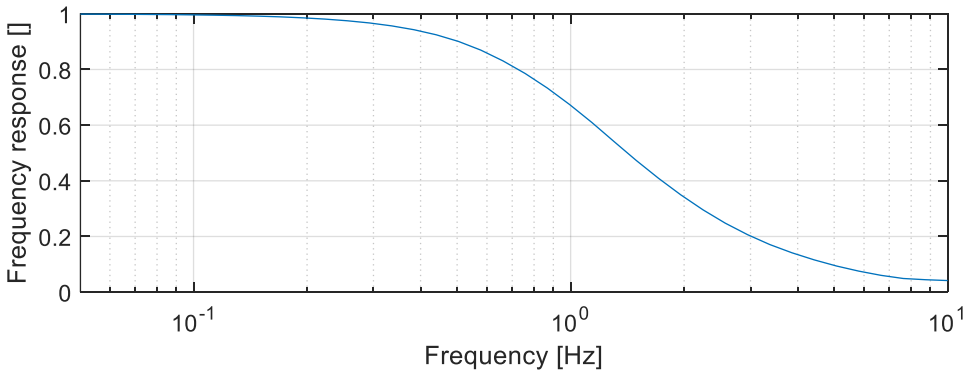

Figure 3.8 Example of frequency response amplitude of the pitch angle control loop (pitch angle reference amplitude = 10 degrees, mass = 12 kg)

3.6.3 Thrust control loops

To be able to apply pitching moments to control the pitch angle, it is necessary to control the thrust force from each of the six motors. The six thrust control loops (one for each motor) are implemented as the inner parts of the pitch angle controller in Figure 3.6. Only the two front motors and the two rear motors are used for pitch control as the two central motor does not contribute to pitching moments.

The thrust from each motor is usually not measured directly. Instead, we assume it is possible to measure rpm (angular rate) and can therefore implement a rpm governor for each motor.

The thrust reference for each motor is therefore converted to a corresponding rpm reference using the relation established in 3.3.1. With no power input to the motor, the propeller rpm is reduced due to aerodynamic braking only. No active braking (M<0) is applied. This is the reason for the falling thrust slope in Figure 3.8 being flatter at low rpms. Note that at a given

stationary rpm, the aerodynamic braking moment is exactly the same as the moment applied from the motor. When reducing the motor moment abruptly, the propeller will initially be braked by the same moment as applied by the motor just before.

A simple PD-controller with thrust as the reference variable and motor torque as control input was implemented. A feedforward of the stationary torque required for the reference rpm reduces the load on the PD-loop.

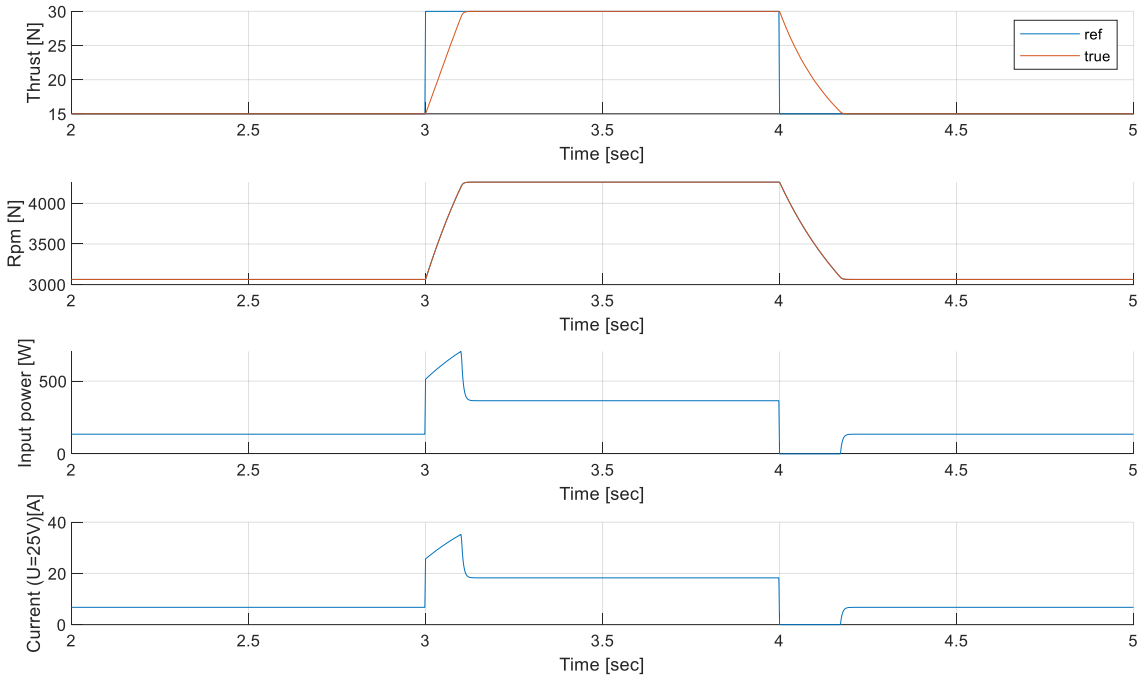

Figure 3.9 Example of motor and thrust data for a thrust reference step input

3.7 Simulation results – time domain

In the simulations in this chapter, all the mass changes are done by altering the mass of the center body of the drone, not the underslung payload. This does change the moment of inertia of the drone somewhat, but not as much as if the payload weight was changed.

The wind disturbances used as test inputs in this chapter is not intended to represent a realistic wind condition. Single step inputs, as well as stochastic series of step inputs should be regarded as extreme cases used to gain a basic understanding of wind rejection in a multirotor drone.

3.7.1 Open loop – wind step example

In this first example, the position controller is not active. The reference pitch angle is always set to zero, so the attitude is locked and the drone is always leveled. The drone is therefore accelerated due to the wind (drag force), and the ground referenced velocity will eventually reach the wind speed (in this case 15 m/s). As the drag model is always the same, increasing the mass will just reduce the acceleration level.

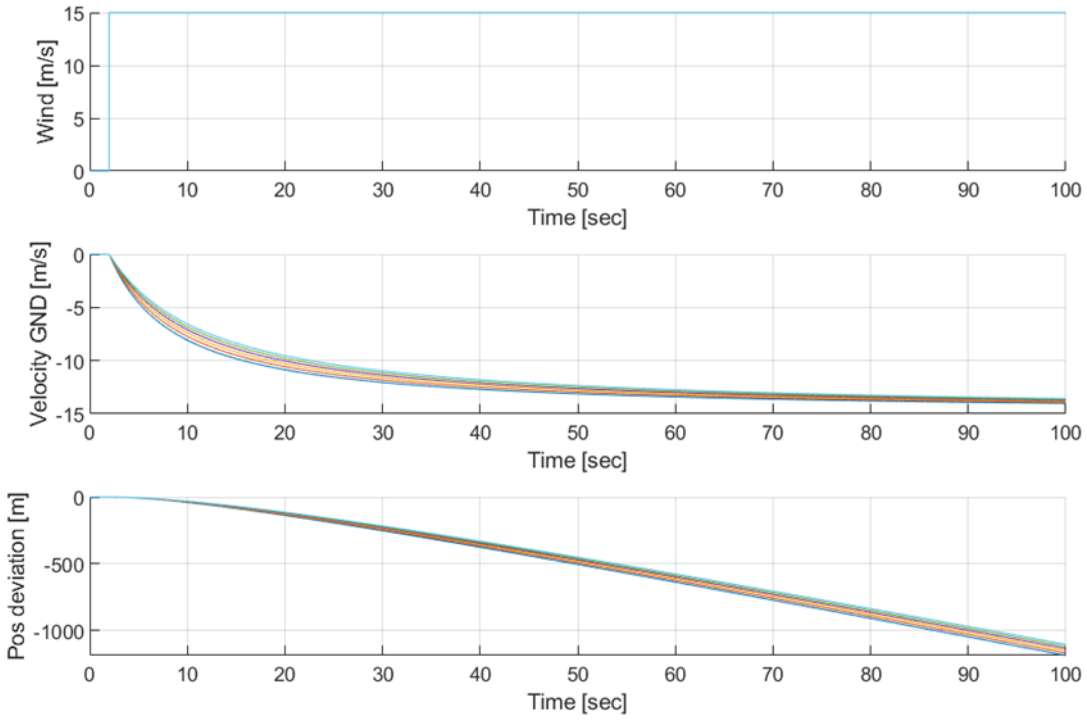

Figure 3.10 Wind step response with no active position controller (open loop). Mass = [10 11 12 13 14 15] kg. (Light blue = 15 kg, dark blue = 10 kg).

3.7.2 Wind modeled as step input – closed loop

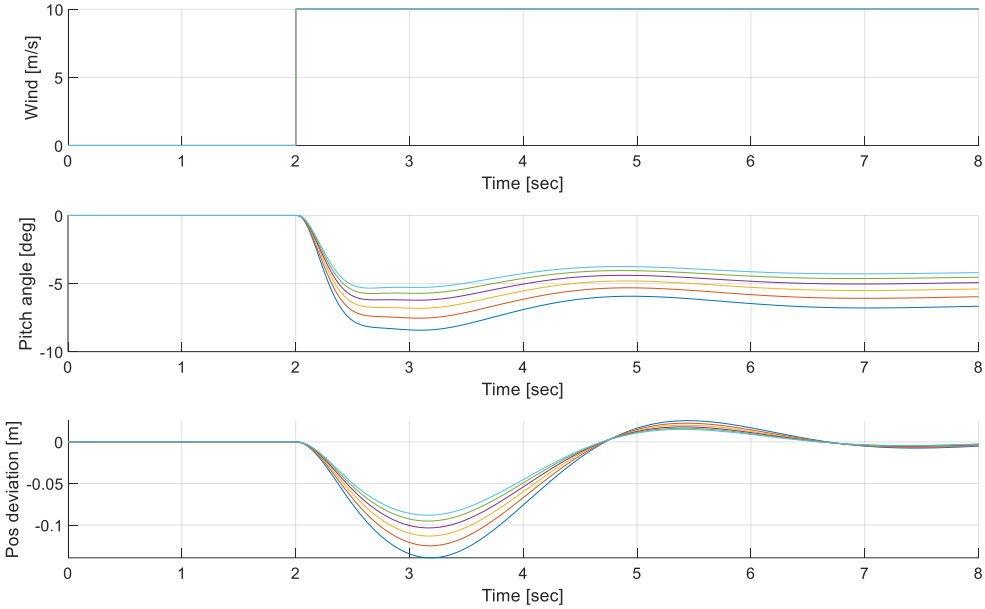

Figure 3.11 Response to wind step input = 10 m/s at t=2.0. Mass = [10 11 12 13 14 15] kg. (Light blue = 15 kg, dark blue = 10 kg).

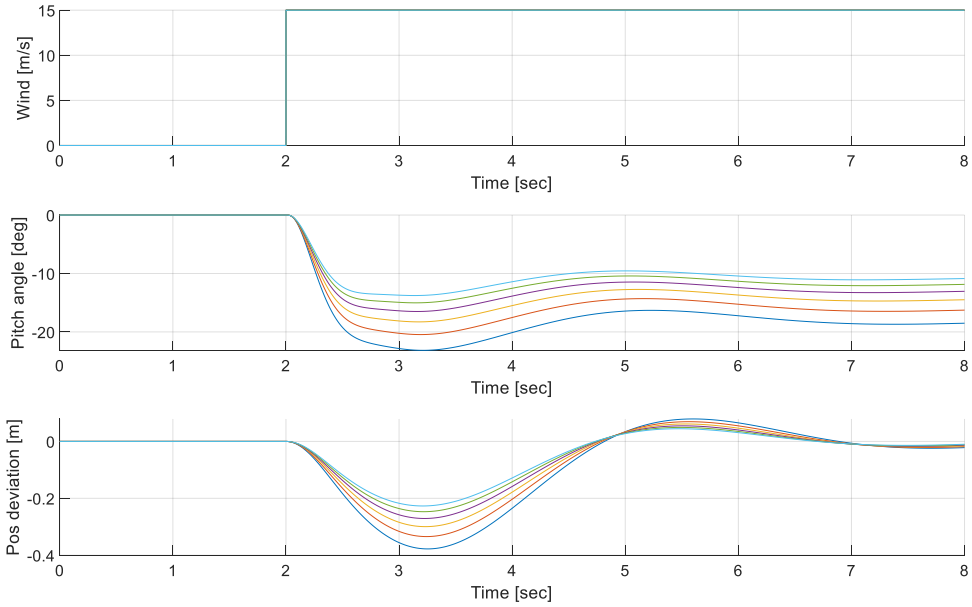

Figure 3.12 Response to wind step input = 15 m/s at t=2.0. Mass = [10 11 12 13 14 15] kg. (Light blue = 15 kg, dark blue = 10 kg).

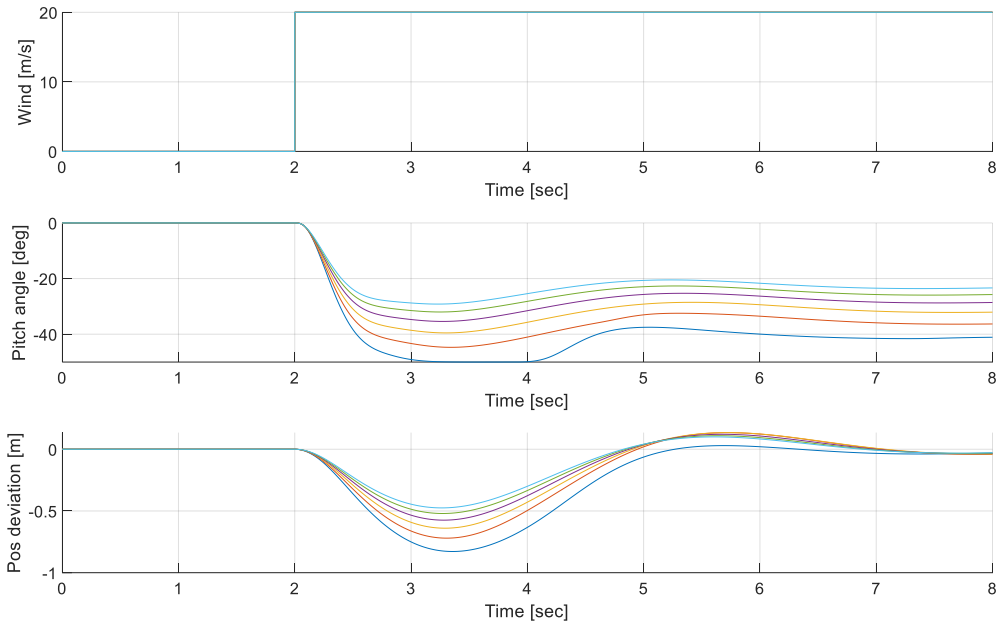

Figure 3.13 Response to wind step input = 20 m/s at t=2.0. Note pitch angle saturation when m=10kg. Mass = [10 11 12 13 14 15] kg. (Light blue = 15 kg, dark blue = 10 kg).

3.7.3 Wind modeled as short pulse

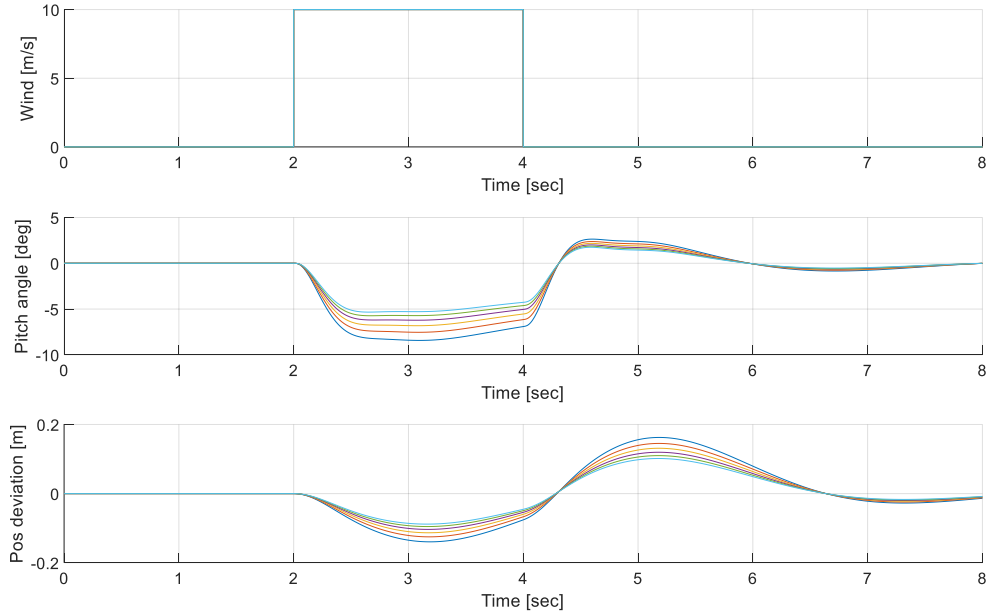

Figure 3.14 Response to wind pulse input = 10 m/s from t=2.0 to t=4.0 sec. Mass = [10 11 12 13 14 15] kg. (Light blue = 15 kg, dark blue = 10 kg).

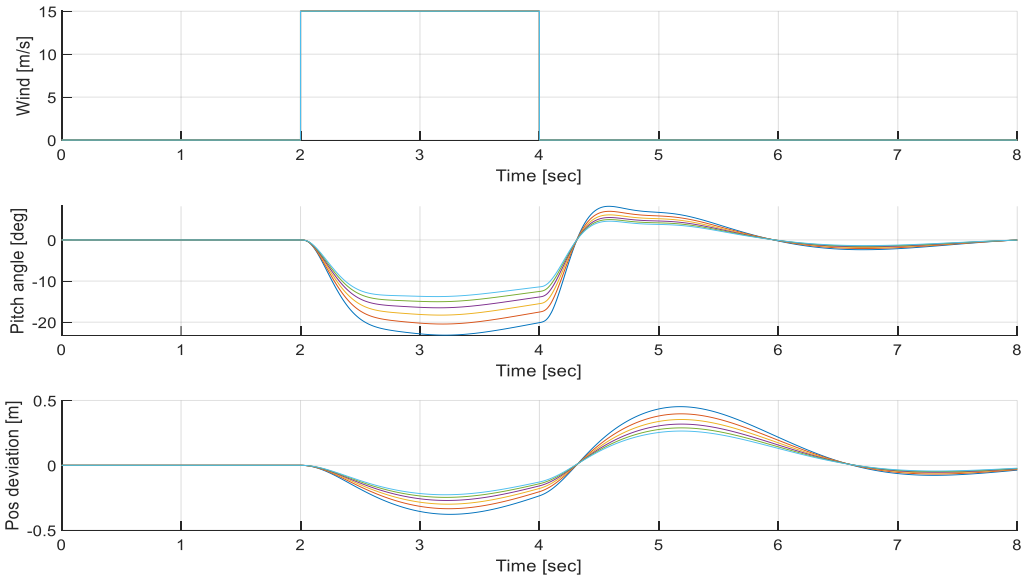

Figure 3.15 Response to wind pulse input = 15 m/s from t=2.0 to t=4.0 sec. Mass = [10 11 12 13 14 15] kg. (Light blue = 15 kg, dark blue = 10 kg).

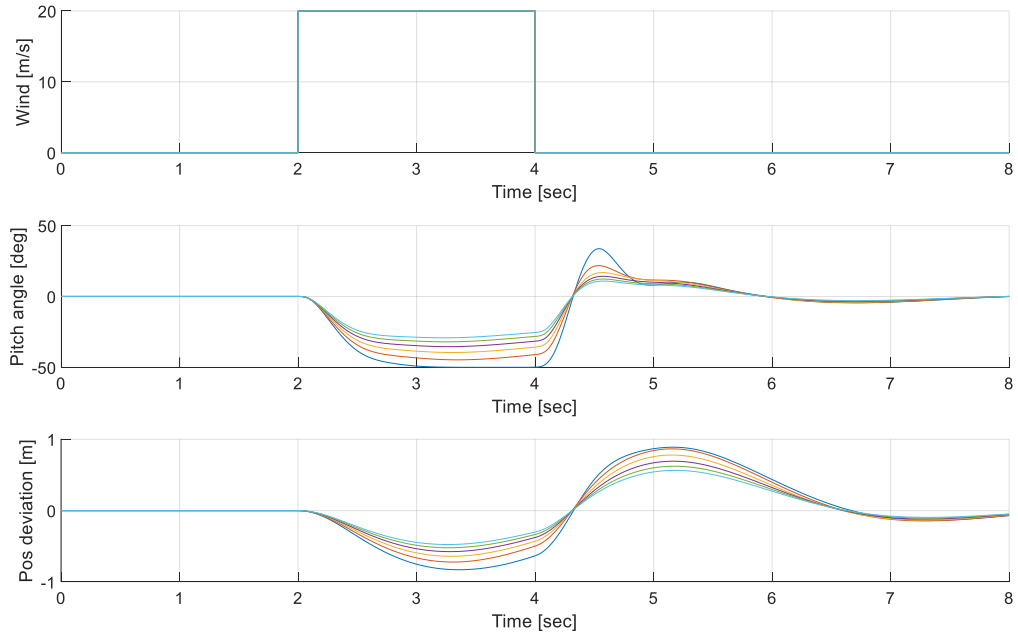

Figure 3.16 Response to wind pulse input = 20 m/s from t=2.0 to t=4.0 sec. Mass = [10 11 12 13 14 15] kg. (Light blue = 15 kg, dark blue = 10 kg).

3.7.4 Stochastic gusting wind

In this example the wind is modeled as a series of consecutive step inputs. The time between the steps is uniformly distributed $\Delta t_{next} \epsilon [0 \rightarrow 3\ sec]$. The wind velocity at the corresponding time step is uniformly distributed $v_{w\_next} \epsilon [-20\ m/s \rightarrow 20\ m/s]$

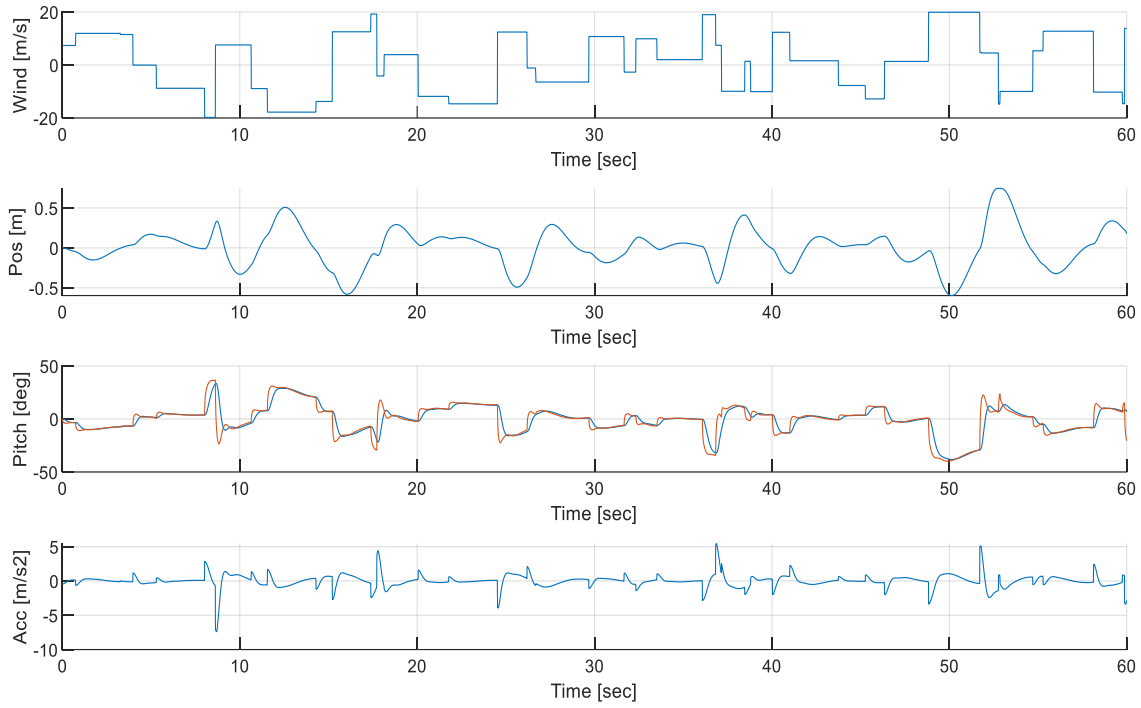

Figure 3.17 *Wind response when the drone is exposed to a stochastic series of step inputs (mass = 12kg). The pitch reference (red) is shown together with the true pitch angle.*

3.7.5 Wind modeled as chirp signal

As a transition from studying the wind response in the time domain to the frequency domain analysis in the next chapter, the drone was exposed to a chirp signal with constant amplitude and varying frequency. In this example, the drone mass was m =12kg.

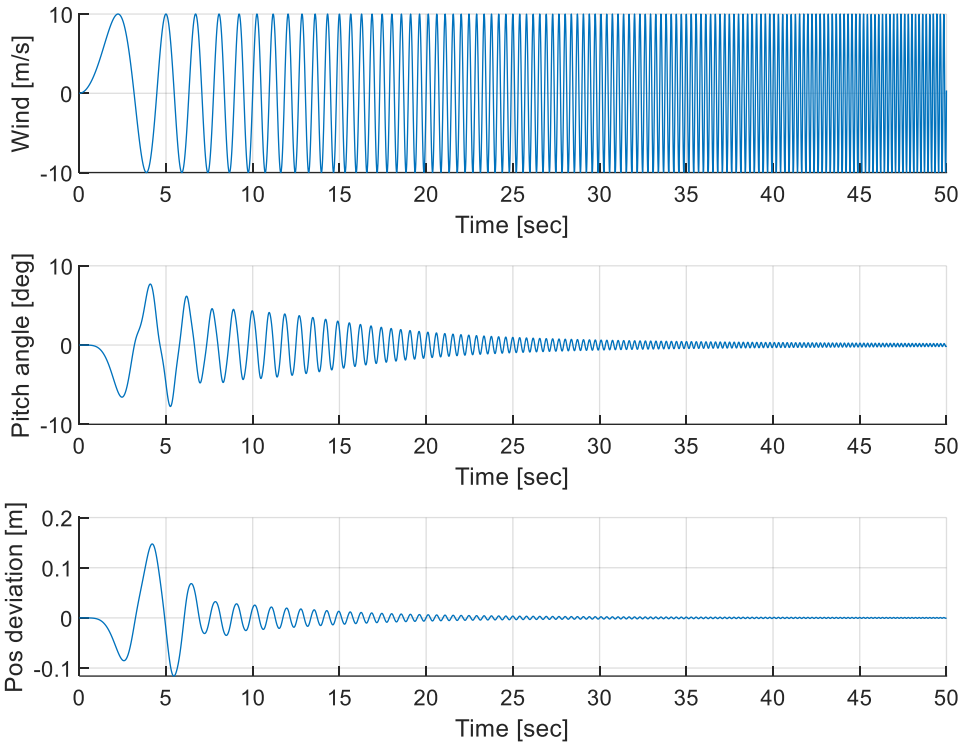

Figure 3.18 Response to wind modeled as a chirp signal. Mass $m = 12kg$.

3.8 Simulation results – frequency domain

In this chapter, the frequency response was not found analytically but through a series of simulations using sinusoidal wind inputs with variable frequency and constant amplitude. The wind inputs has an offset that makes it vary between 0 m/s and a positive maximum value.

The position displacement shown on the frequency response plot y-axis is the peak to peak position variation being comparable to wind input varying between e.g 0 to 6 m/s.

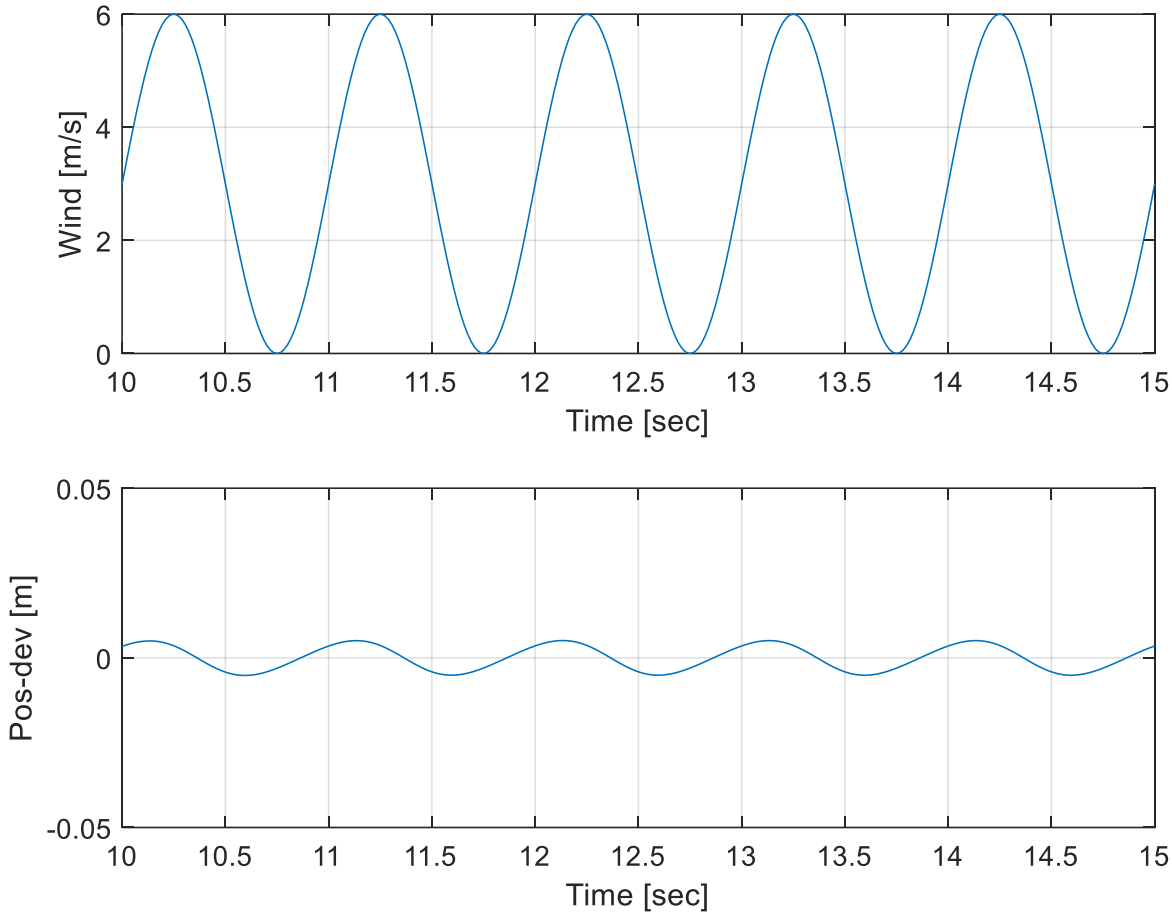

Figure 3.19 Example of simulation @ frequency 1Hz, showing comparable wind input signal and position deviation response. The frequency response analysis was performed by simulations at different frequencies.

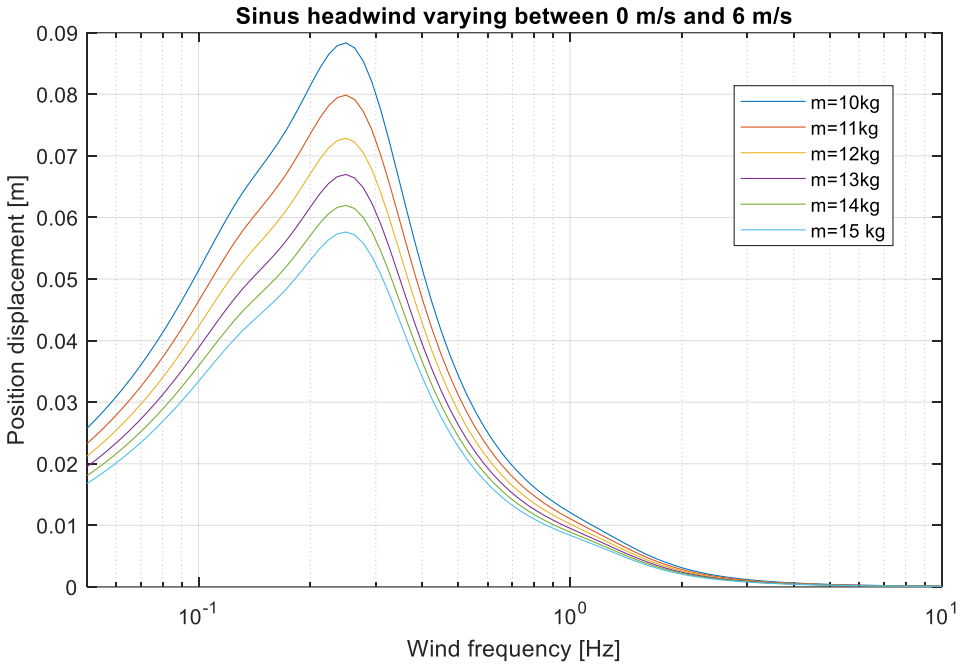

Figure 3.20 Position displacement (p-to-p) for sinusoidal headwind varying between 0 and 6 m/s. Mass = [10 11 12 13 14 15] kg. (Light blue = 15 kg, dark blue = 10 kg).

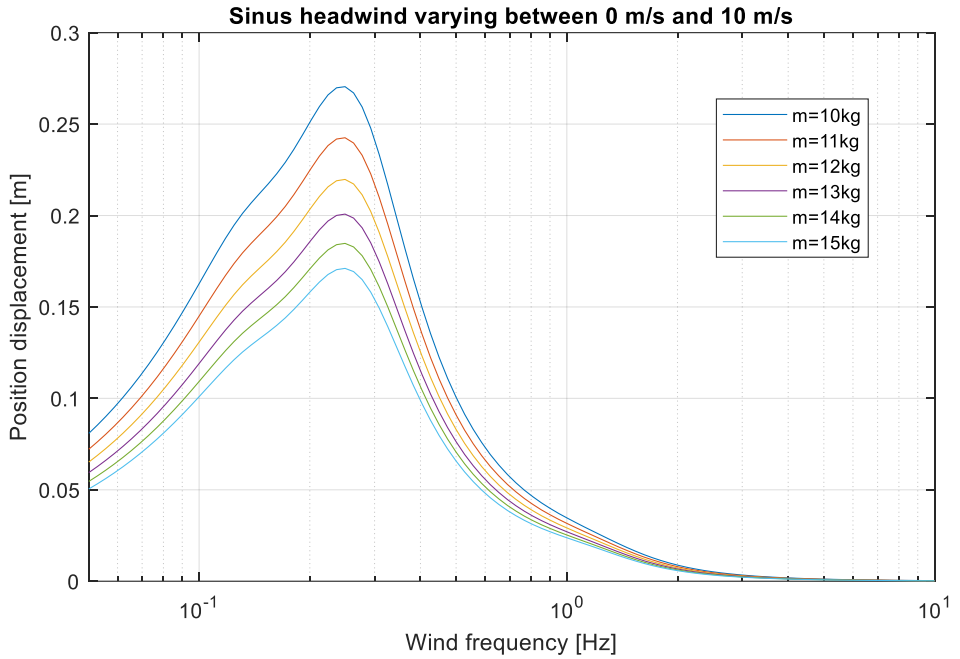

Figure 3.21 Position displacement (p-to-p) for sinusoidal headwind varying between 0 and 10 m/s. Mass = [10 11 12 13 14 15] kg. (Light blue = 15 kg, dark blue = 10 kg).

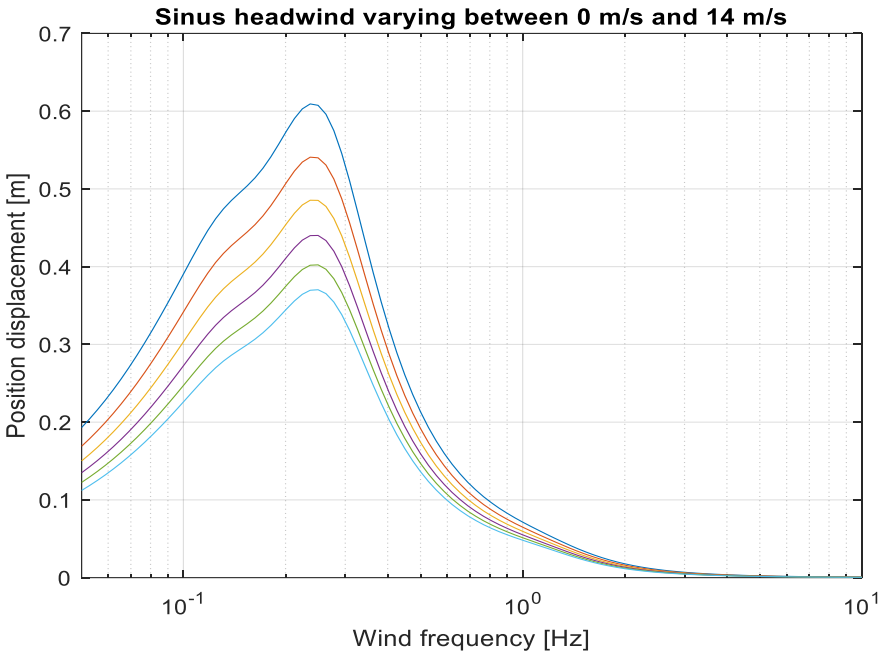

Figure 3.22 *Position displacement (p-to-p) for sinusoidal headwind varying between 0 and 14 m/s. Mass = [10 11 12 13 14 15] kg. (Light blue = 15 kg, dark blue = 10 kg).*

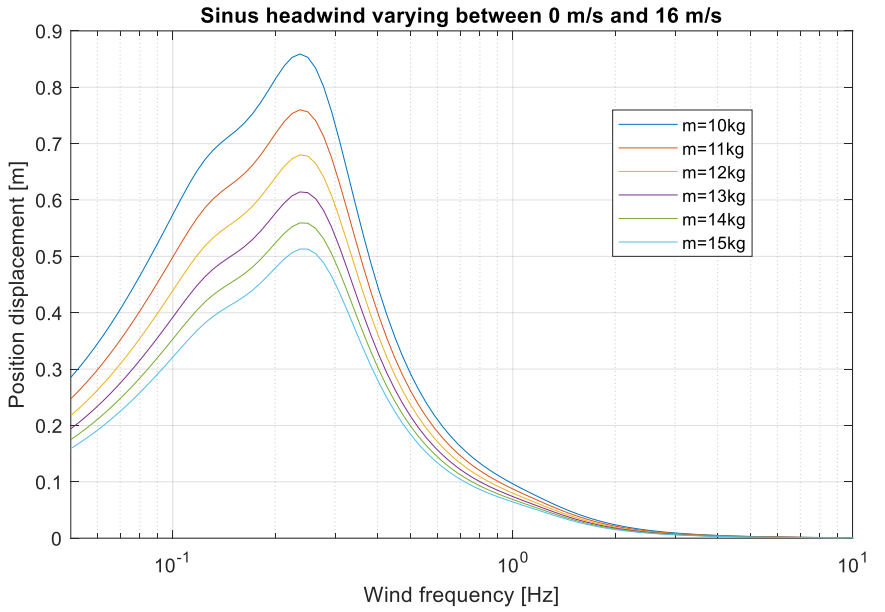

Figure 3.23 *Position displacement (p-to-p) for sinusoidal headwind varying between 0 and 16 m/s. Mass = [10 11 12 13 14 15] kg. (Light blue = 15 kg, dark blue = 10 kg).*

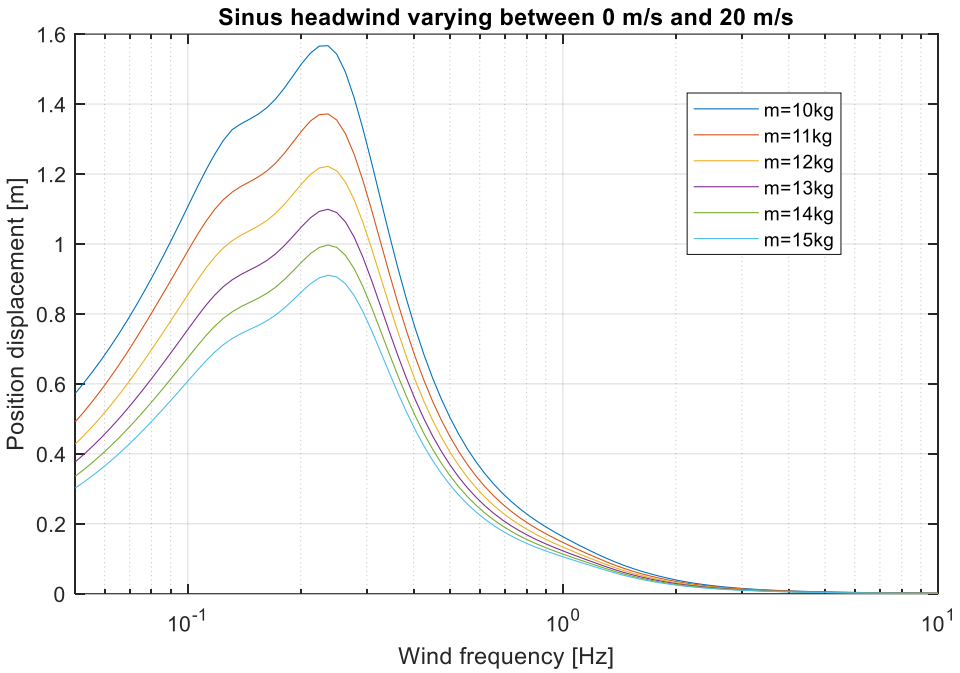

Figure 3.24 *Position displacement (p-to-p) for sinusoidal headwind varying between 0 and 20 m/s. Mass = [10 11 12 13 14 15] kg.* *(Light blue = 15 kg, dark blue = 10 kg).*

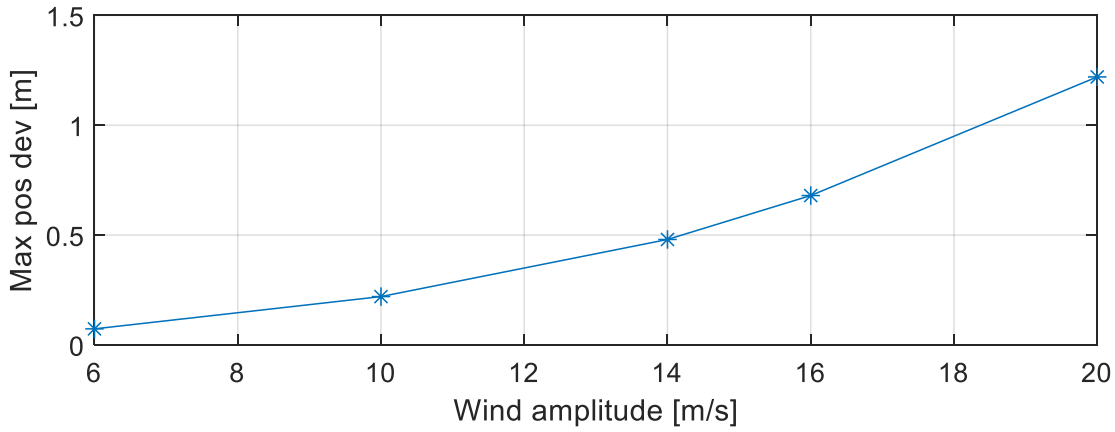

Figure 3.25 *Max position deviation (p-to-p) (@ resonance) as a function of wind amplitude (mass = 12 kg)*

As described in chapter 2, the transition from the sum of forces to position displacement can be expressed as:

$$p_h = \frac{1}{m}\iint (F_h - F_{wind})dt \qquad (3.23)$$

$$p_h(s) = \frac{1}{ms^2}(F_h(s) - F_{wind}(s)) \qquad (3.24)$$

$$p_h(j\omega) = \frac{1}{m(j\omega)^2}(F_h(j\omega) - F_{wind}(j\omega)) \qquad (3.25)$$

At frequencies well above the bandwidth of the pitch angle controller, the term $F_h(j\omega) \to 0$. At these higher frequencies, the shape of the frequency response curve is then dominated by the term $\frac{1}{m(j\omega)^2}$. The frequency response curves are inversely proportional to mass and the frequency squared at higher frequencies.

3.8.1 Acceleration frequency response

In previous chapters, the position deviations as a function of wind frequency, wind amplitude and drone mass have been presented. It might also be of interest to have a closer look at the frequency response of the horizontal accelerations.

The example in Figure 3.24 shows the acceleration frequency response for wind varying from 0-10 m/s. The highest response is found at a frequency of approximately 1.3 Hz. Note that the bandwidth of the pitch angle control loop was found to be 0.9 Hz. So the maximum acceleration response occurs at a frequency where the wind force canceling effect of the pitch angle control loop has been greatly reduced.

At even higher frequencies, the control system has almost no effect and the frequency response is leveling off at values being mostly a function of drag and mass.

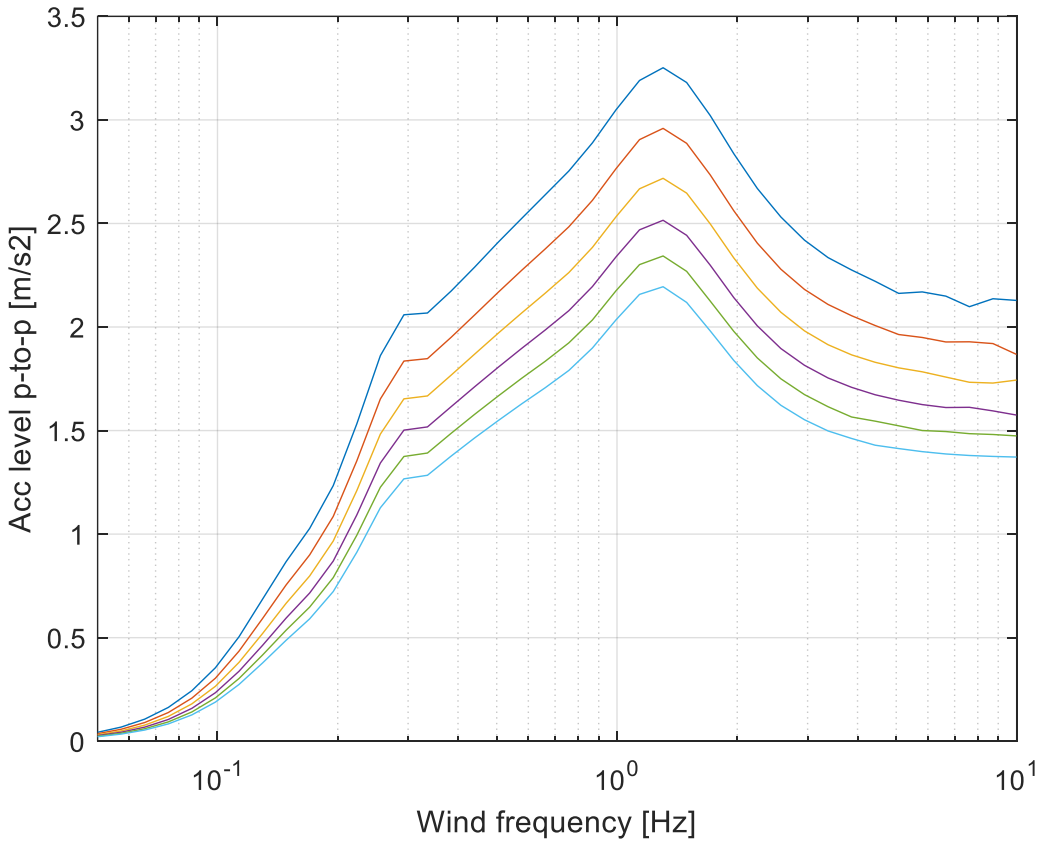

Figure 3.26 Acceleration frequency response when wind is varied between 0-10 m/s. Acceleration level shown is peak to peak variations being comparable to the 0-10 m/s wind variation. The maximum acceleration level felt by the drone at a given frequency is therefore half of what is shown in the figure.

4 Conclusion

The result of this study relies on a set of assumptions, and changing these will impact the numbers presented. Therefore, the study should be regarded as qualitative more than quantitative.

The most important uncertainties are associated with:

- Drag estimation
- Propeller thrust in general, and especially as a function of relative wind speed and drone pitch angle
- Tuning of the control system and no auto adaptation to changing mass or moments of inertia

The study shows however, as expected and experienced during real world drone experiments, that a multirotor drone has a very good suppression of gusting wind. The drone is a high mass density object, and the gust response is therefore very different from a fixed wing airplane.

At very low wind frequencies, (e.g constant wind) the integral term in the position control loop ensures that that the position deviation is very small. At frequencies well above the pitch angle control bandwidth, drone mass and the double integration from force to position effectively dampens the resulting position deviation. Between the very low and higher frequencies, there are resonance frequencies where the position deviation is larger.

An increase in mass is beneficial to the wind suppression in general, both due to the low pass filtering effects and due to the fact that a heavy drone needs to be tilted less to counter the wind forces.

However, if the increased mass also contributes to a significantly increased moment of inertia (this is usually the case), the pitch angle response will suffer and so will the wind suppression performance. An increase in weight of center-mounted batteries will therefore have a different effect than increasing the weight of an underslung payload. In general, if a drone is loaded with a heavy underslung payload, its behavior will become more sluggish, especially if the control system is not auto-adaptive or retuned to the new working conditions. If the increased mass leads to saturation of the motors, controllability and stability of the drone will also suffer.

The best dynamic wind suppression characteristics will in general be found in drones having:

- Low drag coefficient
- Relatively heavy

- Mass being as centered as possible for low inertial moments

The analysis also shows that a drone similar to the Matrice 600 has very little position response to wind disturbances at frequencies above 1-2 Hz. This means that in further experimental work, wind measurements or wind predictions with a higher time resolution than this is of little use.

References

[1] Balchen et.al: “Reguleringsteknikk”, Institutt for reguleringsteknikk, NTNU, 2016

[2[http://www.aerospaceweb.org/question/aerodynamics/q0078.shtml

[3] https://en.wikipedia.org/wiki/Parallel_axis_theorem

Nomenclature

CG = center of gravity

G_{pc} = transfer function for position controller

G_{θ} = transfer function from pitch angle reference θ_{ref} to pitch angle θ

G_F = transfer function from pitch angle θ to horizontal thrust force F_h

θ = drone pitch angle

θ_{ref} = pitch angle reference

a_h = horizontal acceleration (ground referenced)

v_h = horizontal velocity (ground referenced)

v_{air} = air speed felt by the drone

p_h = horizontal position

m = drone mass

F_h = horizontal component of thrust force

F_t = total thrust force

D = drag force due to relative air speed

σ = air density

S = reference area

$\dot{\omega}_{prop}$ = propeller angular acceleration

ω_{prop} = propeller angular velocity

θ_{wc} = pitch angle that in theory will exactly cancel the wind force

About FFI

The Norwegian Defence Research Establishment (FFI) was founded 11th of April 1946. It is organised as an administrative agency subordinate to the Ministry of Defence.

FFI's mission

FFI is the prime institution responsible for defence related research in Norway. Its principal mission is to carry out research and development to meet the requirements of the Armed Forces. FFI has the role of chief adviser to the political and military leadership. In particular, the institute shall focus on aspects of the development in science and technology that can influence our security policy or defence planning.

FFI's vision

FFI turns knowledge and ideas into an efficient defence.

FFI's characteristics

Creative, daring, broad-minded and responsible.

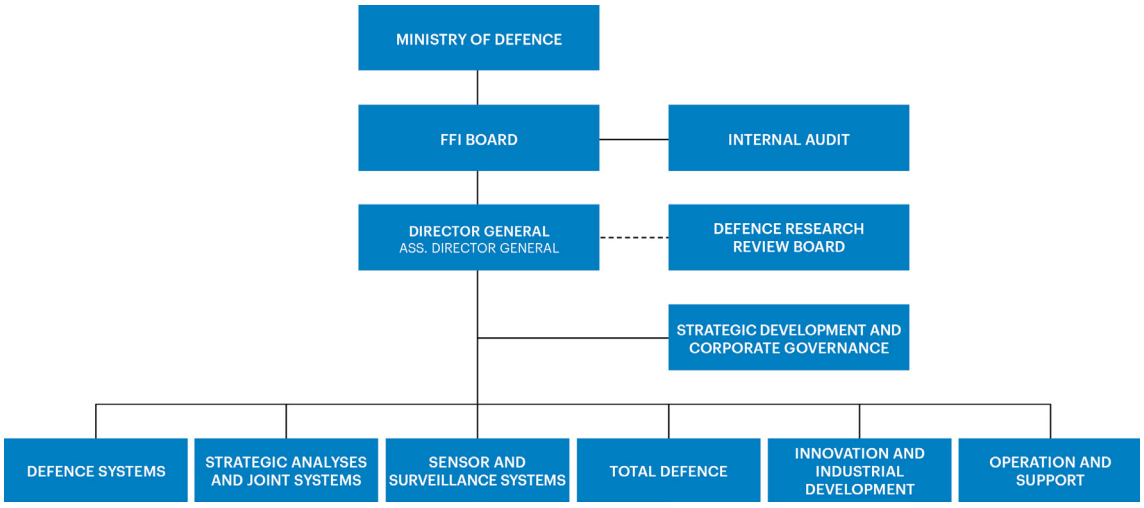

Forsvarets forskningsinstitutt (FFI)
Postboks 25
2027 Kjeller

Besøksadresse:
Kjeller: Instituttveien 20, Kjeller
Horten: Nedre vei 16, Karljohansvern, Horten

Telefon: 91 50 30 03
E-post: post@ffi.no
ffi.no

Norwegian Defence Research Establishment (FFI)
PO box 25
NO-2027 Kjeller
NORWAY

Visitor address:
Kjeller: Instituttveien 20, Kjeller
Horten: Nedre vei 16, Karljohansvern, Horten

Telephone: +47 91 50 30 03
E-mail: post@ffi.no
ffi.no/en